

High Contrast Imaging of the Close Environment of HD 142527

VLT/NaCo adaptive optics thermal and angular differential imaging

J. Rameau¹, G. Chauvin¹, A.-M. Lagrange¹, P. Thebault², J. Milli¹, J.H. Girard³, and M. Bonnefoy⁴

¹ Institut de Planétologie et d'Astrophysique de Grenoble, UJF, CNRS, 414 rue de la piscine, 38400 Saint Martin d'Hères, France
e-mail: julien.rameau@obs.ujf-grenoble.fr

² LESIA-Observatoire de Paris, CNRS, UPMC Univ. Paris 06, Univ. Paris-Diderot, 92195, Meudon, France

³ European Southern Observatory, Alonso de Cordóva 3107, Vitacura, Santiago, Chile

⁴ Max Planck Institut für Astronomie Königstuhl 17, D-69117 Heidelberg, Germany

Received 01 June 2012 ; accepted 06 August 2012

ABSTRACT

Context. It has long been suggested that circumstellar disks surrounding young stars may be the signposts of planets, and still more since the recent discoveries of embedded substellar companions. The planet-disk interaction may create, according to models, large structures, gaps, rings or spirals, in the disk. In that sense, the Herbig star HD 142527 is particularly compelling as, its massive disk displays intriguing asymmetries that suggest the existence of a dynamical perturber of unknown nature.

Aims. Our goal was to obtain deep thermal images of the close circumstellar environment of HD 142527 to re-image the reported close-in structures (cavity, spiral arms) of the disk and to search for stellar and substellar companions that could be connected to their presence.

Methods. We obtained high contrast images with the NaCo adaptive optics system at the Very Large Telescope in L'-band. We applied different analysis strategies to probe the presence of extended structures or point-like sources using both classical PSF-subtraction and angular differential imaging.

Results. The circumstellar environment of HD 142527 is revealed at an unprecedented spatial resolution down to the sub arcsecond level for the first time at $3.8 \mu\text{m}$. Our images reveal important radial and azimuthal asymmetries which invalidate an elliptical shape for the disk as previously proposed. It rather suggests a bright inhomogeneous spiral arm plus various fainter spiral arms. We also confirm an inner cavity down to 30 AU and two important dips at position angles of 0 and 135 deg. The detection performance in angular differential imaging enables the exploration of the planetary mass regime for projected physical separations as close as 40 AU. The use of our detection map together with Monte Carlo simulations sets stringent constraints on the presence of planetary mass, brown dwarf or stellar companions as a function of the semi-major axis. They severely constrain the presence of massive giant planets with semi-major axis beyond 50 AU, i.e. probably within the large disk's cavity that radially extends up to 145 AU or even further outside.

Key words. stars : T Tauri, Herbig Ae/Be - stars : individual : HD 142527 - protoplanetary disks - instrumentation : adaptive optics

1. Introduction

Since the discovery of the first exoplanet (Mayor & Queloz 1995) around the solar-like star 51 Pegasi, more than 760 have been detected so far using different observing techniques, from radial velocity measurements, photometric transit, microlensing to direct imaging. These discoveries reveal a great diversity of planetary systems in terms of physical properties (atmosphere and interior) and environment (single or multiple planets around single stars, in a circumstellar disk or even circumbinary planets). A new paradigm about the formation, structure and composition of planets is emerging, wider than what we have learned so far from the Solar System. Moreover, most of the known detected giant planets orbit within 5 AU owing to the detection biases of radial velocity and transit techniques. The statistical properties of this population of close-in planets, the period-mass distribution, the planet-metallicity correlation together with the densities of Hot Jupiter interiors (Udry & Santos 2007; Mayor et al. 2011) favor a formation mechanism by core

accretion followed by gas capture (CA hereafter, Pollack et al. 1996).

At wider orbits, the distribution of giant planets is less well known. However, the discoveries of planetary mass companions to young, nearby stars in direct imaging (AB Pic b, Chauvin et al. 2005; RXJ 1609 b, Lafrenière et al. 2008), and further more around Fomalhaut (Kalas et al. 2008) and HR8799 (Marois et al. 2008, 2010) challenge the CA model. This scenario suffers from exceedingly long timescales and low disk surface density at large separations. Alternative scenarios could operate at wide orbits, either combined with CA such as planet-planet scattering (Crida et al. 2009) and outward planetary migration (see for instance Mordasini et al. 2012) or alternative formation processes must be invoked like gravitational instability (GI hereafter Cameron 1978) or stellar binary mechanisms. These formation processes should lead to different physical and orbital distributions of giant planets (Boley 2009; Dodson-Robinson et al. 2009). Hence, new discoveries are needed to understand planet formation at all orbits.

The technique of direct imaging technique also offers the possibility to detect giant planets in circumstellar disks to directly study the planet-disk interaction and even dynamically constrain the planets's mass (Chiang et al. 2009; Lagrange et al.

* Based on observations collected at the European Organization for Astronomical Research in the Southern Hemisphere, Chile, ESO : run 087.C-0299A.

2012a). Indirect signs of planetary formation such as clumps, gaps, holes and spiral arms (see a review in Papaloizou et al. 2007) have been probably already observed within several proto-planetary disks (e.g AB Aur, Fukagawa et al. 2004; TCha, Huéramo et al. 2011; Andrews et al. 2011SAO 206462, Muto et al. 2012).

In this context, using high contrast imaging, we have observed the close environment of the star HD 142527, known to host an extended proto-planetary disk. HD 142527 is a Herbig star Waelkens et al. (1996), classified as a F6IIIe (Houk 1978). The Hipparcos measurement has been revisited by van Leeuwen (2007) leading to a parallax of $\pi = 4.29 \pm 0.98$ mas, i.e. $d = 233^{+69}_{-43}$ pc. However, HD 142527 has been identified as a member of the star-forming region Sco OB2-2 (Acke & van den Ancker 2004) or Upper Centaurus Lupus (de Zeeuw et al. 1999) hence the distance would be $d = 145 \pm 15$ pc in both cases. We choose to adopt this latter distance since we consider the identification of the membership more reliable. The age and the mass of the star are also matter of debate since Fukagawa et al. (2006, F06 hereafter) derived an age of 2.2^{+3}_{-2} Myr and $M = 1.9 \pm 0.3 M_{\odot}$ from its stellar UV/optical luminosities and isochrone (from Palla & Stahler 1999) whereas Verhoeff et al. (2011) found an age of ≈ 5 Myrs and $M = 2.2 \pm 0.3 M_{\odot}$ based on a new estimation of the stellar luminosity and pre main sequence isochrones (from Siess et al. 2000). Finally, Pecaute & Mamajek (2010) discussed the age of F-type members of the Sco-Cen OB association and estimated it to be in the range [5; 20] Myr. We therefore considered an age between 2 and 20 Myr for further analysis. The Table 1 summarizes the stellar properties of HD 142527. This system, resolved by F06 in NIR and Fujiwara et al. (2006) in IR, presents a circumstellar disk quite unusual with unprecedented infrared excess ($F_{IR}/F_{\star} = 0.98$ and $F_{NIR}/F_{\star} = 0.32$, Dominik et al. 2003) compared to other Herbig stars. Evidence of grain growth (deduced from thermal and scattered light observations) together with the high level of crystallinity (MIDI observations, van Boekel et al. 2004, and NIR spectrum, Honda et al. 2009) reveal that the outer disk is characterized by highly-processed dust. Moreover, F06 notes the presence of a spiral arm, a prominent cavity up to ≈ 150 AU, two asymmetric facing arcs within the disk and measured a stellar offset of ≈ 20 AU with respect to the center of the disk. Models have been computed to fit the infrared excess, the geometry of the inner disk and the mineralogy of the dust (Verhoeff et al. 2011). They found a disk cavity between 30 and 130 AU separating an inner disk embedded in a halo and a massive outer disk extended to 200 AU. They conclude that on-going giant planet formation is suggested from the highly evolved status of the disk surrounding HD 142527.

To get a more accurate view of the close-in structures (cavity, spiral arms) of the disk at unprecedented spatial resolution and to search for stellar and substellar companions that could be connected to their formation, we carried out VLT/NaCo observations at L' band using angular differential imaging (ADI hereafter). We present the observing strategy and the data reduction in Section 2, the fine structures and the geometry of the cavity and of the outer disk in Section 3, finally the detection performance and the constraints on the presence of giant planets in Section 4.

2. Observations and Data reduction

2.1. Observing strategy and observing conditions

HD 142527 was observed on July 29th, 2011 under good seeing conditions in the course of the thermal imaging survey of

Table 1. HD 142527 properties

Parameters	
RA (J2000)	+15 : 56 : 41.88
DEC (J200)	-42 : 19 : 23.27
Proper motion RA (mas/yr)	-11.2 \pm 0.9
Proper motion DEC (mas/yr)	-24.46 \pm 0.8
Spectral Type	F6IIIe
K (mag)	4.98 \pm 0.02
Distance (pc)	145 \pm 15 ^a
Age (Myr)	2 – 20
Mass (M_{\odot})	2.2 \pm 0.3 ^a

Notes. ^(a) Based on new estimation of the stellar luminosity in Verhoeff et al. 2011.

56 young and dusty stars (Rameau et al. 2012, in prep). We used the VLT/NaCo (Lenzen et al. 2003; Rousset et al. 2003) high contrast adaptive optics system and imager in angular differential imaging mode (ADI, Marois et al. 2006). The L'-band ($\lambda_0 = 3.8 \mu\text{m}$, $\Delta\lambda = 0.62 \mu\text{m}$) was used with the L27 camera (platescale ≈ 27.1 mas/pixel). Twilight flats were obtained for calibration. A first set of short unsaturated exposures with a neutral density filter (ND-Long) was acquired to serve as calibration for the point-spread function (PSF) and for the relative photometry and astrometry calibrations. A second set of saturated exposures, without the neutral density filter, was obtained to image the environment of HD 142527 with a high dynamic range. Both sequences were composed of various offset positions on the detector for background subtraction and bad or hot pixels removal. A windowing mode (512 \times 514 pixels) was chosen to allow short exposure times (DIT) and favor the temporal sampling using the NaCo cube mode. The parallactic angle variations ($\Delta\pi = 44.4$ deg) are reported on Table 2, together with the exposure time, the number of frames per cube (NDIT), the number of cubes (Nexp) and the observing conditions. The star HD 181296 (A0, K = 5.01 mag), that was used as reference for classical PSF-subtraction, was observed with the same observing strategy during the same night.

2.2. Data processing

All images were reduced using the pipeline developed for ADI observations at the Institut de Planétologie et d'Astrophysique de Grenoble (see Lagrange et al. 2010; Bonnefoy et al. 2011; Delorme et al. 2012; Chauvin et al. 2012). All data were homogeneously flat-fielded and sky-subtracted; bad and hot pixels were also cleaned from the images. The data were then recentered and bad quality images were removed from the cubes. The result was a master cube containing all individual cleaned and recentered frames, along with their parallactic angles.

To probe the inner part of the environment of HD 142527, we used different PSF-subtraction strategies either adapted for the detection of faint extended structures or to search for point-like features. These four methods are described below:

1. Spatial filtering combined with simple derotation (referred as nADI). An azimuthal average of the radial profile is estimated and subtracted from each image of the master cube, followed by a derotation and mean-stacking. A further step consists in an additional median filtering (fnADI hereafter).
2. Classical ADI (cADI). The median of all individual reduced images is subtracted from the master cube, followed by a derotation and mean-stacking of individual images.

Table 2. Observing Log of HD 142527 in L'-band with and without the neutral density (ND), as well as for the reference star HD 181296.

Star	Date	UT-start/end	DIT (s)	NDIT	Nexp	π -start/end ^a (°)	\langle Airmass \rangle^b	$\langle\bar{\omega}\rangle^b$ (arcsec)	$\langle\tau_0\rangle^b$ (ms)
HD 142527 (ND)	07/29/2011	23:49/23:52	0.2	80	10	-15.4/-12.9	1.05	0.76	1.6
HD 142527	07/29/2011	23:59/01:03	0.2	100	129	-7.9/36.5	1.05	0.55	2.1
HD 181296	07/29/2011	03:23/04:27	0.2	100	124	-5.5/23.3	1.15	1.34	0.9

Notes. ^(a) π refers to the parallactic angle at the start and the end of observations. ^(b) The airmass, the seeing $\bar{\omega}$ and the coherence time τ_0 are estimated in real time by the AO system and averaged here over the observing sequence.

- The LOCI algorithm (Lafrenière et al. 2007). The residuals are minimized for each image using linear combinations of all data to derive the PSF contribution at a given location in the image. For LOCI, we considered optimization regions of $N_A = 300$ PSF cores, the radial-to-azimuthal width ratio $g = 1$, the radial width $\Delta r = 1$ and $2 \times FWHM$, and a separation criteria of 1.0 and $1.5 \times FWHM$. A slightly revisited version of LOCI was applied with an estimation of the reference that does not take into account the contribution of the region of interest (referred as to mLOCI, see Lagrange et al. 2012b; Milli et al. 2012).
- Finally, classical PSF-subtraction (e.g. Mawet et al. 2009). The observations were not designed to perform such reduction afterwards but we found that HD 181296 was observed in our survey (Rameau et al. 2012, in prep.) 2 hours later with the same parallactic angle conditions. We therefore used it as a reference (see table 2 for the observing conditions). To optimally subtract the PSF to HD142527's mastercube, we first selected science and reference frames with similar parallactic angle variations (covering a total of 26 deg). From each individual science frame, the closest reference one in terms of parallactic angle (within 0.3 deg) was subtracted, after recentering and flux rescaling. This step enables the optimization the subtraction of the telescope+instrument static-speckles. The PSF-subtracted science frames are then deroated and mean-stacked. Different methods were applied to estimate the flux scaling factor between HD 142527 and HD 181296 : 1) by applying the same scaling to all frames, 2) by determining an individual scaling factor for each individual frame considering the total flux between the science and reference frames, 3/ using two independent part of the image (below 0.7 and above 1.5 of radii, to exclude the brightest part of the disk) to derive an individual scaling factor for each individual frame. The best result was validated according to visual check.

These four PSF-subtraction methods allowed us to reach optimal detection performance at all separations, identify biases and non-physical structures. Although ADI (as with high-pass filtering) processes are well adapted for point-like detections, they are not for axisymmetric disks with low inclination (in the present case $i \simeq 30^\circ$) since the disks are heavily self-subtracted (Milli et al. 2012 submitted). However they still enable the detection of non-axisymmetric structures and sharp edges in the disk. On the other hand, nADI, low pass filtering and PSF-reference subtraction reveal large scale features, both in terms of separation and size. Careful checks have been done with the Airy ring patterns while interpreting the observed structures. The results of these four methods are discussed below in the context of the disk morphology and of the presence of close companions in the environment of HD 142527.

3. The circumstellar disk around HD 142527

3.1. Disk morphology

Our results on the disk morphology of HD 142527 are mainly based on the classical PSF-reference subtraction method, more adapted to the conservation of faint axisymmetric structures with low inclination. The complexity of this method is the determination of the flux scaling factor to avoid the creation of artifacts. After various tests, we ended up with the fact that there is not an optimal and unique scaling factor for all radii. We therefore tried to subtract the PSF-reference with a radial scaling factor at each 1 pixel-wide annuli or at each few pixels-wide annuli. The results were not convincing because of the asymmetric and high contrasted structures leading to over-subtracted regions. Unresolved diffuse material seems to highly contribute to the PSF-flux observed at L' in addition to the observed structures further away (see details below).

Nonetheless, it is evident from all images to probe fine highly contrasted structures. The Figure 1 and Figure 2 show the images of HD 142527 reduced using the classical PSF-reference subtraction and fnADI, cADI, mLOCI procedures within a reduced FoV of $4.2'' \times 4.2''$. However, the photometry of the features remains sensitive to the choice of the scaling factor. The images reveal new complex, non-axisymmetrical structures in addition to those previously reported (F06; Fujiwara et al. 2006; Ohashi 2008). We discuss the main features below.

- *Spiral arms.* One of the main results from F06 reveals two elliptical facing arcs towards the East-West directions and a displacement of the star with respect to the center of a fitted ellipse on the disk. Our data do not confirm this architecture but rather suggest spiral shapes. The fnADI image (Figure 2, left) remains the most adapted to see the following features. From PA = 170 ± 4 deg to PA = 264 ± 2 deg, the arm goes closer to the central star, from $1.17 \pm 0.04''$ to $0.95 \pm 0.02''$, with a higher bending at 226 deg. A remarkable feature appears at PA = 265 ± 1 deg : the spiral arm shifts closer to the star of $0.11 \pm 0.02''$. This represents a strong rupture to the axisymmetric structure suggested by F06. When going North, the arm moves away (up to $0.91 \pm 0.03''$). We estimate the arm width of about $0.43''$ for PA = 227 deg after PSF-reference subtraction with $sf = 2.2$ (without data binning).

Considering the East part of the disk (see Figure 2, right), the separation increases from North West ($0.87 \pm 0.03''$) to South East ($1.11 \pm 0.05''$). This spiral arm is not homogenous, showing peaks and dips. fnADI, cADI and LOCI highlight this inhomogeneity by revealing blobs. We also estimate the arm width for PA = 47 deg of about $0.38''$.

Slightly further out of the main western spiral arm, we detect

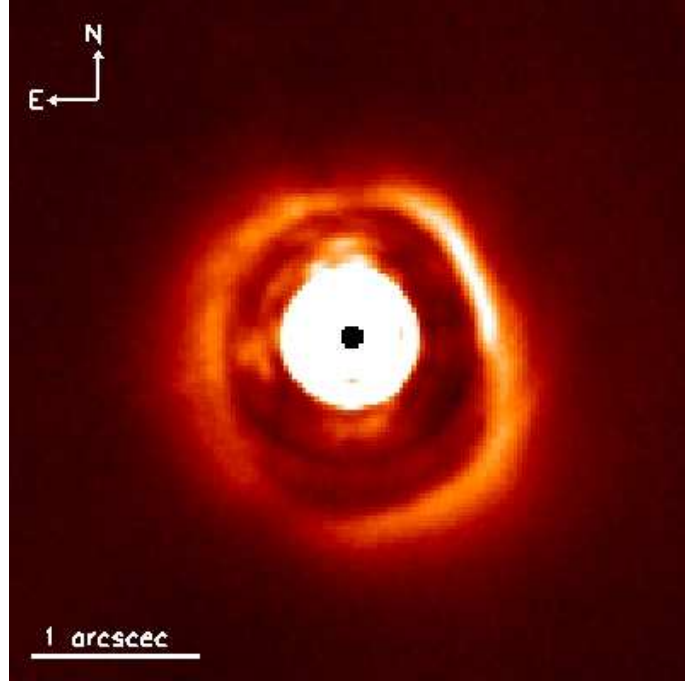


Fig. 1. HD142527 L' image with a $4.2'' \times 4.2''$ field of view reduced with the PSF-reference technique and a scaling factor of 2.2. This factor seems to subtract better the close-in flux without an over subtraction of the most external parts. North is up, East is left ; flux scale is linear.

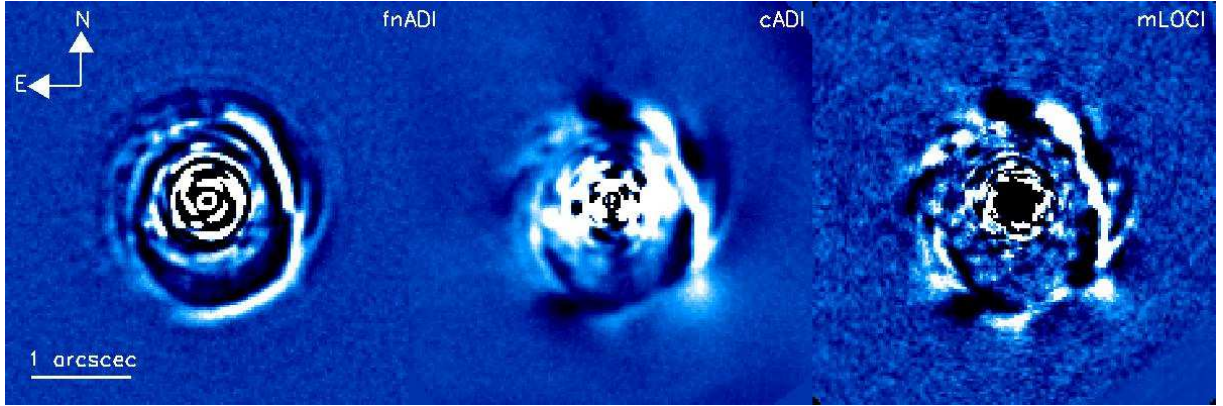


Fig. 2. HD142527 L' images with a $4.2'' \times 4.2''$ field of view. North is up, East is left. **Left :** fnADI using a high-pass filtering. **Middle :** cADI. **Right :** mLOCI using a mask to exclude the disk. Note that the linear flux scale is different for each panel to reveal all structures.

at least two spiral arms which are born out at $(1.1 \pm 0.1'', PA = 242 \pm 3 \text{ deg})$ and $(1.01 \pm 0.04'', PA = 261 \pm 3 \text{ deg})$ and move away while going to North. These spirals show up very well in cADI and mLOCI reduced images, up to the 9σ confidence level within the LOCI ones. However, the intensity is not uniform along these arms and their width are narrow compared to the ones in the PSF-reference images. These effects due to ADI processing are detailed in Milli et al. (2012, submit.).

Further out from the star, we confirm the presence of a spiral arm between $(\approx 1.71'', \approx 243 \text{ deg})$ and $(\approx 1.88'', \approx 302 \text{ deg})$ as observed in K and H-band in F06. As mentioned in previous papers at shorter wavelengths, we confirm that this arm is fainter with increasing wavelength.

- *The brightness asymmetry between the West and East directions* It clearly comes out from all images that the West side of the disk is brighter than the East one. This observa-

tion confirms the previous one by F06. At the same separation, the Western arm is brighter than the Eastern one up to $\approx 2 \text{ mag/arcsec}^2$ (see for instance the SBD profile in Figure3), bottom).

- *The prominent cavity.* We confirm this cavity already observed by F06. It is re-detected with an outer edge at $0.87 \pm 0.06''$, i.e. $\approx 126 \text{ AU}$ at 145 pc , along $PA = 227 \text{ deg}$. F06 presented the cavity to be elliptical and later simulations took into account this geometry. However, it is clear that the outer edge of the cavity differs from an ellipse. In particular, it is much more pronounced into the South West and extends further up to 145 AU when going South, as a consequence of the spiral shape described earlier. Considering the East part, the edge is located at $0.73 \pm 0.02''$, $PA = 64 \text{ deg}$, i.e. $\approx 106 \text{ AU}$.
- *Two azimuthal dips.* We confirm the presence of two big dips, detected at North ($PA \in [351 \pm 2; 9 \pm 5] \text{ deg}$ and South-East

($PA \in [148 \pm 6; 164 \pm 2]$ deg). The presence of point-like sources in these two dips is discussed below (Section 4.2).

3.2. Surface brightness distribution

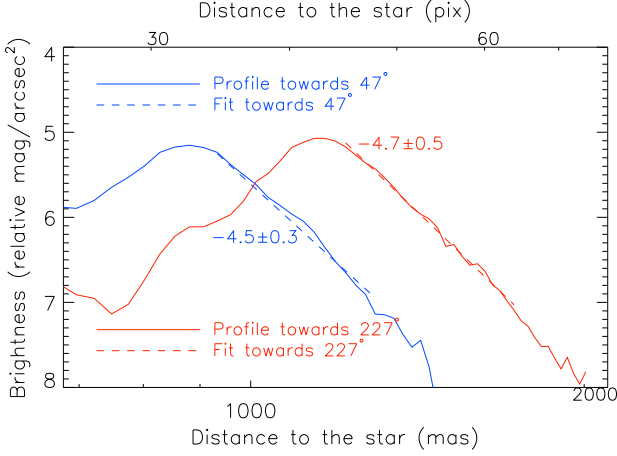


Fig. 3. Observed radial surface brightness distribution on HD 142527 L' PSF-reference subtracted image with a scaling factor of 2.2 towards the extended part of the disk (47–227 deg). Dashed lines corresponds to fitted straight line between 0.9'' and 1.3'' for $PA = 47$ deg and between 1.2'' and 1.8'' for $PA = 227$ deg.

We extracted the surface brightness distribution (SBD) of the HD 142527's disk using the classical PSF-subtracted image. We derived the radial profile to evaluate the extension, the slopes of the outer disk and the amplitude of features observed in the images towards several PA in 1 pixel-wide annulus. The resulting SBD toward the largest extension of the disk (i.e. $PA = 47$ & 227 deg) are shown on Figure 3. The slope was measured between 0.87'' and 1.3'' for $PA = 47$ deg and between 1.2'' and 1.8'' for $PA = 227$ deg. We found that the SBD follows a simple power law with a slope of $\simeq -4.6$. The mass of gas in the disk being poorly constrained (Ohashi 2008), if the circumstellar disk around HD 142527 is gas-free disk, such an outer distribution would be indicative of the dust dynamics dominated by radiation pressure effects (e.g. Thébaud & Wu 2008).

To investigate the brightness asymmetry between the West and East side of the disk, we used the GraTeR code (Augereau et al. 1999) to simulate, as a preliminary step, the disk as a ring following a radial volumic distribution of grains : $((r/r_0)^{-2\alpha_{in}} + (r/r_0)^{-2\alpha_{out}})^{-0.5}$. We chose $r_0 = 145$ AU, $\alpha_{out} = -\alpha_{in} = -3.7^1$, the disk height scale $\xi = 1$ AU at r_0 , a gaussian vertical profile with $\gamma = 2$, a linear disk flaring with $\beta = 1$ and an inclination of $i = 30$ deg. The disk width thus obtained is 0.48'', which is larger than the one measured for $PA = 227$ deg, but 0.36'' if we assume $i = 45$ deg. We simulated the disk with different scattering properties, from $g = 0$ (isotropic) to $g = 0.5$. An anisotropy with $g = 0.25$ could explained the flux ratio of 2 with $i = 30$ deg and also $g = 0.15$ with $i = 45$ deg. However, such configuration could not explain the geometry asymmetry by itself. It might be created either by an offset of the disk center

¹ The distribution slopes have been chosen to match the SBD slopes measured on the data.

or by an asymmetry between the forward scattering branch and the backward scattering one.

3.3. Role of a close-in binary companion?

Billier et al. (2012) have recently detected a close-in low-mass star companion candidate, using the NaCo/Sparse Aperture Mode (Tuthill et al. 2010). This candidate has a predicted mass of $0.1 - 0.4 M_{\odot}$ for a physical projected separation of 88 ± 5 mas ($\simeq 13$ AU). This candidate should rely at $\simeq 3.3$ pixels with a contrast of 5.2 mag with the primary in our NaCo ADI/L'-band images. However, we did not detect any point source or insight of this companion due to the very small inner working angle and thus numerous residual speckles. If confirmed with a second epoch observation, the companion could be responsible for the non-axisymmetric features of the circumstellar disk around HD 142527. Indeed, the secular perturbations from a central binary are known to create transient, outward propagating spiral structures in a circumbinary disc (see for instance the numerical investigations of Artymowicz & Lubow 1994; Bate 2000; de Val-Borro et al. 2011). The extent, evolution and longevity of these spiral structures depend on several parameters, such as the binary mass ratio and orbital eccentricity but also the spatial structure and density of the gas component of the disc. The detailed study of their evolution in the specific case of HD 142527 requires advanced numerical modeling that clearly exceeds the scope of the present paper and is left to future investigations.

4. Additional companions around HD 142527

4.1. Detected point-like sources

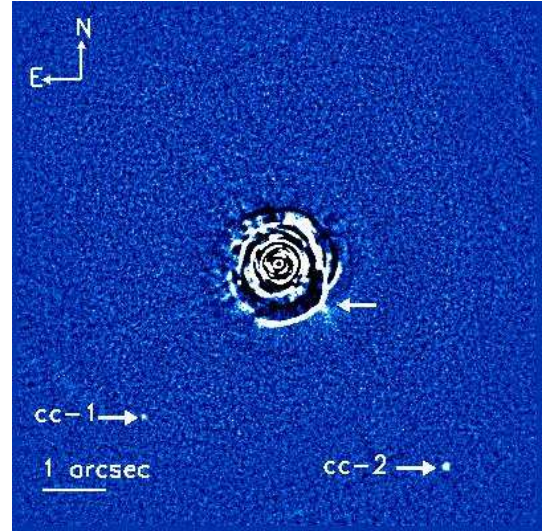


Fig. 4. fnADI with median filtering image of HD 142527 with a $11'' \times 11''$ FoV. The arrows indicate candidate companions ; cc-1 and cc-2 are confirmed as background sources whereas the third one is likely an ADI artefact created by the disk. Note that the negative parts (black) close to the disk result from the azimuthal averaging.

We looked for point-like sources in a complete FoV of $19'' \times 19''$, obtained after considering all fields observed during the dithering pattern. We confirm the presence of two faint point sources (the companion candidates cc-1 and cc-2, see Figure 4),

Table 3. Relative Astrometry and Photometry of the point-sources detected around HD 142527.

Candidate	UT Date	Instrument	Separation (")	PA (deg)	$\Delta L'$ (mag)	Status
cc-1	04/06/2004	Subaru/CIAO	4.23 ± 0.02	140.8 ± 0.3		
	07/29/2011	VLT/NaCo	4.168 ± 0.008	138.9 ± 0.2	13.3 ± 0.3	Background
cc-2	04/06/2004	Subaru/CIAO	5.56 ± 0.02	218.5 ± 0.3		
	07/29/2011	VLT/NaCo	5.371 ± 0.009	219.9 ± 0.2	11.9 ± 0.2	Background

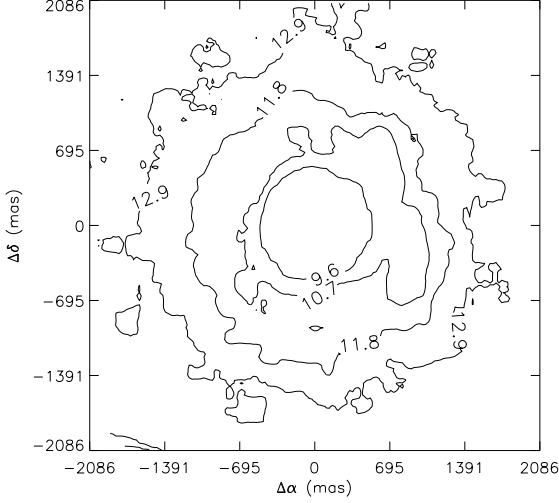


Fig. 5. 2D contrast in L' at 5σ for point-like sources from LOCI reduction around HD 142527.

already detected by F06. Combining the Subaru/CIAO dataset from 2006 and our NaCo observations, we confirm the background nature of these two sources. Their relative astrometry and photometry derived at each epoch are reported in Table 3.

At closer separations within $2''$, various point-like structures are detected in the cADI and LOCI images (see Figure 1). Owing to the low inclination of the disk, the ADI processing may create artifacts, either extended ones (holes) or point-like (in the case of abrupt changes in the shape of extended structures). The bright signal located at $1.3''$ and $PA = 227.5$ deg) is for example created by the elbow’s shape of the south-western part of the disk. Consequently, we do not detect any unambiguous companion candidates within $2''$.

4.2. Detection limits

To compute the ADI detection performance with LOCI and cADI, the flux loss of the ADI processing was estimated by injecting fake planets of given separation and contrast in a cube with empty frames (and in the data master cube for LOCI). The full pipeline was run. By comparing the injected fluxes to the recovered ones, we could derive the flux losses as a function of the separation. The second step was to estimate the noise in the residual maps using a sliding box of 9×9 pixels. The 5σ detection limits were then derived by correcting the noise from the flux loss and applying a normalization using the unsaturated PSF. We visually checked and confirmed the detection limits by inserting fake planets with several expected contrasts at several separations. The 2D-contrast map obtained with LOCI is shown on Figure 5. We are sensitive to point-like sources with a contrast of $\Delta L' = 10.5$ mag at 700 mas ($\Delta_{proj} = 101$ AU) and 12.5 mag at

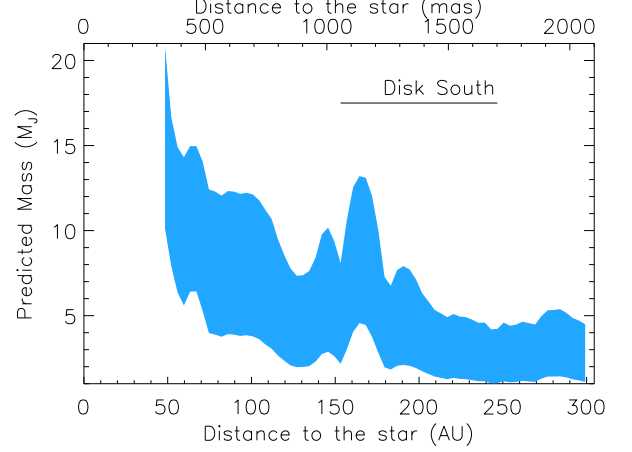


Fig. 6. Detection limits expressed in Jupiter mass towards the South direction with cADI (similar performance as LOCI). The aqua zone displays the explored masses between 2 and 20 Myr since the age of the star is not well established. The position of the disk as been added towards the same PA.

1500 mas (similar performance was obtained with cADI). They correspond to planetary masses of $6.5 M_{Jup}$ and $2.5 M_{Jup}$ at 101 and 218 AU, respectively, using the predictions of the COND03 evolutionary models (Baraffe et al. 2003) for an age of 5 Myrs. We also explored the performance towards the northern prominent dip of the disk and along the South direction within the large southern cavity. The 1D predicted mass vs projected separation (only one case is shown because similar performance is obtained in both directions) towards the South is reported in Figure 6. Considering the large uncertainty on the age of the star, whereas the Herbig status and gas presence are evidence for young age, the explored masses between 2 and 20 Myr are plotted on the Figure. We do not detect any planets more massive than $5 M_{Jup}$ in the northern disk’s dip and $4 M_{Jup}$ in the southern cavity. Careful considerations have to be taken since the detection limits might be overestimated close to the edges of the disk and to the spiral arms due to the disk impact in ADI processes (see Milli et al. 2012).

4.3. Detection probabilities

To set constraints on the physical characteristics of unseen giant planets or brown dwarfs that could be responsible for several disk structures, we used the Multi-purpose Exoplanet Simulation System (the MESS code Bonavita et al. 2012). Such analysis initiated by (Kasper et al. 2007) has been extensively done up to now, especially to constrain the giant planet population at wide orbits. We first assumed a population of planets coplanar with the disk by fixing the inclination to 30 deg. The code creates a planet population using a uniform (mass and semi-major axis) grid. We

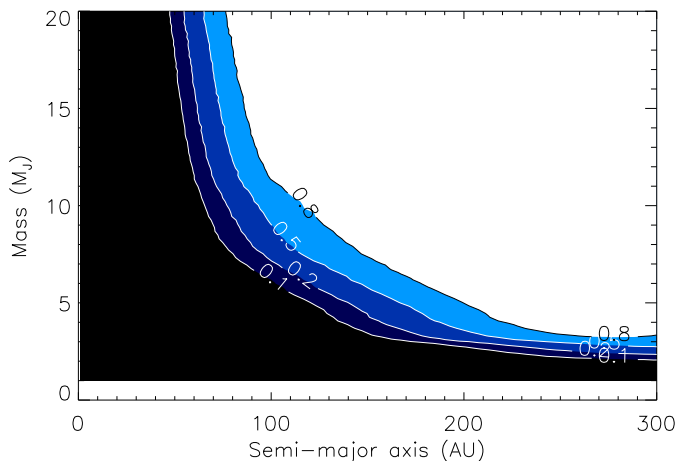


Fig. 7. Detection probability map of a faint companion around HD 142527 as a function of mass and semi-major axis. The constraint of $i = 30$ deg has been set to orbital properties of the generated planets. This was calculated using the LOCI 2D detection limits within a $4.2'' \times 4.2''$ FoV.

explored a parameter space of semi-major axis ranging between 1 and 500 AU and of masses between 1 and $20 M_{\text{Jup}}$, resulting in a final grid of 100×100 points. For each point, the code has generated $N_{\text{gen}} = 10000$ orbits and computed the projected position of the planet at the time of the observation. Using the 2D-contrast maps converted in terms of masses (using the COND model's predictions, Baraffe et al. 2003) and projected physical separations, the code finally checked the detectability of each simulated planet and determined their detection probability given their masses and semi-major axis (see Figure 7). Our NaCo observations set constraints for planetary mass-objects down to semi-major axis $a \geq 40$ AU and do not completely explore the large cavity between the outer spiral structures of HD 142527 and the inner disk located at less than 30 AU. The detection probabilities unambiguously exclude the presence of massive planets with $M \geq 9 M_{\text{Jup}}$ and $M \geq 5 M_{\text{Jup}}$ for semi-major axis of $a \geq 130$ AU and 200 AU, respectively. To test the impact of inclination in our simulations, we ran simulations for $i \in [10, 50]$ deg, considering that a third component will not be necessarily coplanar if the binary companion detected by Biller et al. (2012) is confirmed. The detection probabilities do not change significantly our previous results.

5. Summary and concluding remarks

Our observations using VLT/NaCo adaptive optics thermal and angular differential imaging reveal the disk surrounding HD 142527 at an unprecedented spatial resolution down to the subarcsecond level. The disk shows a vast and asymmetric cavity between 30 AU and 145 AU as well as two important dips towards North and South East. We also resolve a bright and inhomogeneous spiral arm towards the West direction, several fainter spiral arms and structured features rather than two elliptical facing arcs as proposed in previous studies. The observations in angular differential imaging allow us to derive unprecedented detection performance of point-sources down to planetary-mass at 40 AU from the star. Monte-Carlo simulations combined with our detection map set stringent constraints on the presence of substellar companions orbiting HD 142527. We exclude the presence of brown dwarfs and massive giant planets

in the outer part of the cavity and the presence of giant planets down to $5 M_{\text{Jup}}$ further out.

The observed structures indicate that the disk is in an active phase of global evolution. We have already discussed the possibility that the binary companion candidate might be highly responsible for the creation of these features. However, other processes can be invoked such as one or more unseen planets under formation in the disk.

Gravitational instability is known to create global spiral modes and in some cases fragmentation. However, given that the gas mass, as well as the surface density had been poorly constrained so far, it is not possible to know if the conditions are favorable for gravitational instability. Type II migration of a high mass planet can also be a mechanism able to produce such structures (e.g. Armitage & Rice 2005) in a gaseous disk. Thus, once again, constraints on the gas properties will allow to exclude or not the type II migration.

While this article was under review Casassus et al. (2012) reported Gemini/NICI Ks and L' observations of the outer part of the HD 142527 circumstellar environment. Given similar performance of NICI and NaCo, it gives us the opportunity to validate the observed features and excluded them to be instrumental or analysis artifacts. They confirmed the presence of several structures : the spiral arms, the asymmetric inner cavity, the two North and South South East dips and the inhomogeneity of the East side. However, we do not confirm in our images the presence of what they called a 'knot' along the North West arm. In their images, we also clearly see the offset of the main arm that we reported towards the West, even if they did not mention this peculiar morphology. Furthermore, they investigated the presence of a $10 M_{\text{J}}$ protoplanet at 90 AU through hydrodynamic simulations to reproduce the morphology of the inner cavity and of the outer disk. Given our detection performance, such a companion would have likely been detected thus ruling out the input parameters of this carving planet. They argued themselves for additional ingredients within the simulations to reproduce all structures for which one single planet cannot explain. Nevertheless, their approach is very interesting and could be improved by taking into account our detection limits to set planet characteristics and the inner binary candidate companion within FARGO simulations.

From the present data, it is rather difficult to identify the cause of the non axisymmetric cavity and spiral arms due to the lack of knowledge on the gas properties. However, we consider that they may be due to at least one bound-embedded object. Further observations and important numerical investigations will be necessary to further test the origin of the highly structured disk of HD 142527.

Acknowledgements. This research has made use of the SIMBAD database and the VizieR service, operated at CDS, Strasbourg, France. We would like to thank M. Bonavita for providing us the MESS code to perform MC simulations. JR also thanks the ESO staff for conducting the observations. We also acknowledge financial support from the French National Research Agency (ANR) through project grant ANR10-BLANC0504-01.

References

- Acke, B. & van den Ancker, M. E. 2004, *A&A*, 426, 151
- Andrews, S. M., Wilner, D. J., Espaillat, C., et al. 2011, *ApJ*, 732, 42
- Armitage, P. J. & Rice, W. K. M. 2005, *ArXiv Astrophysics e-prints*
- Artymowicz, P. & Lubow, S. H. 1994, *ApJ*, 421, 651
- Augereau, J. C., Lagrange, A. M., Mouillet, D., Papaloizou, J. C. B., & Grorod, P. A. 1999, *A&A*, 348, 557
- Baraffe, I., Chabrier, G., Barman, T. S., Allard, F., & Hauschildt, P. H. 2003, *A&A*, 402, 701
- Bate, M. R. 2000, *MNRAS*, 314, 33

- Billier, B., Lacour, S., Juhász, A., et al. 2012, *ApJ*, 753, L38
- Boley, A. C. 2009, *ApJ*, 695, L53
- Bonavita, M., Chauvin, G., Desidera, S., et al. 2012, *A&A*, 537, A67
- Bonnefoy, M., Lagrange, A.-M., Boccaletti, A., et al. 2011, *A&A*, 528, L15+
- Cameron, A. G. W. 1978, *Moon and Planets*, 18, 5
- Casassus, S., Perez M., S., Jordán, A., et al. 2012, *ApJ*, 754, L31
- Chauvin, G., Lagrange, A.-M., Beust, H., et al. 2012, *ArXiv e-prints*
- Chauvin, G., Lagrange, A.-M., Zuckerman, B., et al. 2005, *A&A*, 438, L29
- Chiang, E., Kite, E., Kalas, P., Graham, J. R., & Clampin, M. 2009, *ApJ*, 693, 734
- Crida, A., Masset, F., & Morbidelli, A. 2009, *ApJ*, 705, L148
- de Val-Borro, M., Gahm, G. F., Stempels, H. C., & Pepliński, A. 2011, *MNRAS*, 413, 2679
- de Zeeuw, P. T., Hoogerwerf, R., de Bruijne, J. H. J., Brown, A. G. A., & Blaauw, A. 1999, *AJ*, 117, 354
- Delorme, P., Lagrange, A. M., Chauvin, G., et al. 2012, *A&A*, 539, A72
- Dodson-Robinson, S. E., Veras, D., Ford, E. B., & Beichman, C. A. 2009, *ApJ*, 707, 79
- Dominik, C., Dullemond, C. P., Waters, L. B. F. M., & Walch, S. 2003, *A&A*, 398, 607
- Fujiwara, H., Honda, M., Kataza, H., et al. 2006, *ApJ*, 644, L133
- Fukagawa, M., Hayashi, M., Tamura, M., et al. 2004, *ApJ*, 605, L53
- Fukagawa, M., Tamura, M., Itoh, Y., et al. 2006, *ApJ*, 636, L153
- Hashimoto, J., Tamura, M., Muto, T., et al. 2011, *ApJ*, 729, L17
- Honda, M., Inoue, A. K., Fukagawa, M., et al. 2009, *ApJ*, 690, L110
- Houk, N. 1978, Michigan catalogue of two-dimensional spectral types for the HD stars
- Huélamo, N., Lacour, S., Tuthill, P., et al. 2011, *A&A*, 528, L7
- Kalas, P., Graham, J. R., Chiang, E., et al. 2008, *Science*, 322, 1345
- Kasper, M., Apai, D., Janson, M., & Brandner, W. 2007, *A&A*, 472, 321
- Lafrenière, D., Jayawardhana, R., & van Kerkwijk, M. H. 2008, *ApJ*, 689, L153
- Lafrenière, D., Marois, C., Doyon, R., Nadeau, D., & Artigau, É. 2007, *ApJ*, 660, 770
- Lagrange, A.-M., Bonnefoy, M., Chauvin, G., et al. 2010, *Science*, 329, 57
- Lagrange, A.-M., De Bondt, K., Meunier, N., et al. 2012a, *ArXiv e-prints*
- Lagrange, A.-M., Milli, J., Boccaletti, A., et al. 2012b, *ArXiv e-prints*
- Lenzen, R., Hartung, M., Brandner, W., et al. 2003, in *SPIE*, Vol. 4841, 944–952
- Marois, C., Lafrenière, D., Doyon, R., Macintosh, B., & Nadeau, D. 2006, *ApJ*, 641, 556
- Marois, C., Macintosh, B., Barman, T., et al. 2008, *Science*, 322, 1348
- Marois, C., Zuckerman, B., Konopacky, Q. M., Macintosh, B., & Barman, T. 2010, *Nature*, 468, 1080
- Mawet, D., Serabyn, E., Stapelfeldt, K., & Crepp, J. 2009, *ApJ*, 702, L47
- Mayor, M., Marmier, M., Lovis, C., et al. 2011, *ArXiv e-prints*
- Mayor, M. & Queloz, D. 1995, *Nature*, 378, 355
- Milli, J., Mouillet, D., Lagrange, A. M., et al. 2012, *ArXiv e-prints*
- Mordasini, C., Alibert, Y., Benz, W., Klahr, H., & Henning, T. 2012, *A&A*, 541, A97
- Muto, T., Grady, C. A., Hashimoto, J., et al. 2012, *ApJ*, 748, L22
- Ohashi, N. 2008, *Ap&SS*, 313, 101
- Palla, F. & Stahler, S. W. 1999, *ApJ*, 525, 772
- Papaloizou, J. C. B., Nelson, R. P., Kley, W., Masset, F. S., & Artymowicz, P. 2007, *Protostars and Planets V*, 655
- Pecaut, M. & Mamajek, E. 2010, in *Bulletin of the American Astronomical Society*, Vol. 42, American Astronomical Society Meeting Abstracts #215, #455.30
- Pollack, J. B., Hubickyj, O., Bodenheimer, P., et al. 1996, *Icarus*, 124, 62
- Rousset, G., Lacombe, F., Puget, P., et al. 2003, in *SPIE*, Vol. 4839, 140–149
- Siess, L., Dufour, E., & Forestini, M. 2000, *A&A*, 358, 593
- Thébaud, P. & Wu, Y. 2008, *A&A*, 481, 713
- Tuthill, P., Lacour, S., Amico, P., et al. 2010, in *SPIE*, Vol. 7735
- Udry, S. & Santos, N. C. 2007, *ARA&A*, 45, 397
- van Boekel, R., Min, M., Leinert, C., et al. 2004, *Nature*, 432, 479
- van Boekel, R., Min, M., Waters, L. B. F. M., et al. 2005, *A&A*, 437, 189
- van Leeuwen, F. 2007, *A&A*, 474, 653
- Verhoeff, A. P., Min, M., Pantin, E., et al. 2011, *A&A*, 528, A91
- Waelkens, C., Waters, L. B. F. M., de Graauw, M. S., et al. 1996, *A&A*, 315, L245